Group 20 Urban Search and Rescue Robot

Supporting Document:

This paper considers Lithium Batteries powering an Urban Search and Rescue Robot. The batteries power multiple brushed permanent magnet direct current motors. It is recognised that Urban Search and Rescue Robots are required to operate at a large range of ambient temperatures. The potential implication of the effect on the robot's battery life is an issue that has been assessed to require further research. It was found that temperature does affect Lithium battery life and the behaviour of direct current motors significantly, hence the need for temperature compensation was determined. Since temperature management is expensive and cumbersome, the idea of a software-based model to extend battery life under extreme temperature conditions has been developed. This is novel in the field of mobile robotics. The combination of dynamic battery and direct current motor models presented here contributes to a field of research that has been of increasing interest in recent years. Accurate, online battery state-of-charge determination is of universal interest in any mobile electronics application, an exemplary embodiment of this is the advent of both smartphones and electric vehicles in recent years, where similar models obtained through simulation and iterative model improvements from experimental tests are employed for SOC estimations.

ES410 Technical Paper

A Dynamic Model of the Effect of Ambient Temperature Variations on Lithium Battery Life when Powering Brushed Permanent-Magnet Direct Current Motors

J. Specht (1416924); C. Perera (1312528); T. de Oliveira (1419972); M. Safford (1411064); E. Carman (1431487); B. Vidos (1309358); E. Chotai (1328512)

Funding Organisations:
University of Warwick – School of Engineering
Warwick Manufacturing Group
Catapult; GRP; Mouser; Xilinx; GRM

Abstract:

This paper considers Urban Search and Rescue robots operating under extreme temperature conditions. A dynamic Lithium battery model supplying power to a brushed direct current motor at varying ambient temperatures assuming an initial state-of-charge of one is developed. Both the battery and the motor are described in terms of their equivalent circuits and then simulated at different load and temperature conditions. Variation of internal battery resistance with battery state-of-charge and ambient temperature is shown. Temperature effects on direct current motor winding resistance and inductance are estimated as linear functions. Battery state of charge was shown to vary by about 15.7 percent per 20°C deviation from a 20°C ambient temperature. Furthermore, it was shown that increasing the robot motor torque requirement by 50mNm results in a 14.7 percent increase in battery depletion rate. A practical test of the described model has been carried out and potential causes of arising discrepancies have been identified. It has been shown that a reduction in current draw extends battery life and may increase the reliability of search and rescue missions. The general discharge behaviour of Lithium batteries consisting of fast initial cell voltage drop and a following cell voltage plateau region was verified, and it is expected that extensive iterative system testing and results evaluation with consequent model adjustments may allow the development of a highly accurate algorithm for battery state-of-charge estimation in Urban Search and Rescue Robots. It reliability should be unaffected by ambient temperature.

Keywords: Lithium Battery; DC Motor; State of Charge; Thermal Behaviour; Mobile Robot

1. Introduction:

Urban Search and Rescue (USAR) Robots are required to operate in extreme conditions, for example in reconnaissance missions after structure fires or natural disasters. The design of USAR robot on-board power supplies requires special focus on wide ambient temperature variations. Lithium batteries are energy dense, with densities up to 620Wh kg^{-1}, thus are employed widely in mobile applications, however their cycle life and State-of-Charge (SOC) is highly temperature dependent [1]. In a closed circuit, the Lithium at one electrode combines with the metal-oxide of the other electrode across an electrolyte interface [1]. This gives rise to a current by allowing Lithium ions to pass when the battery is in closed-circuit conditions [2].

$$a\mathrm{Li} + \mathrm{M}_b\mathrm{O}_c \leftrightarrow \mathrm{Li}_a\mathrm{M}_b\mathrm{O}_c$$

The battery has an internal resistance that is temperature dependent [1]. Battery-powered USAR robots often employ brushed permanent magnet direct current motors (BPMDC). To operate at a specific torque, these require a current that varies with temperature [3]. The aim of this paper is to model the effect of wide ambient temperature variations on the SOC of Lithium Polymer batteries powering the electronic system of a USAR robot employing BPMDC motors under varying load torques. Existing battery models are considered and combined with dynamic modelling techniques for DC motors.

The results are then used to develop an algorithm for robot power management in different ambient temperatures to allow on-board battery monitoring and for computationally inexpensive SOC estimations, increased robot mission reliability, in addition to potentially extended battery life.

2. Theoretical Model:

2.1. Battery Model:

A common model for SOC is given by the charge counting equation, Equation 1 [4].

$$SOC = SOC_0 - \int \left(\frac{i_{battery}}{Q_{usable}}\right) dt \qquad (1)$$

This equation uses an initial SOC value, SOC_0, between 0 and 1, calculated through Equation 2 [5] and the battery current, $i_{battery}$ and the usable battery charge, Q_{usable}.

$$SOC_0 = 1 - 0.000442(\Delta T + 0.714932)^2 \qquad (2)$$

$$\Delta T = T_{cell} - T_{amb}$$

An amount dependent on ambient temperature according to ΔT is subtracted from the initial SOC to account for variations in battery capacity caused by ambient temperature, T_{amb}, variations. Equation 2 gives maximum state of charge when battery cell temperature, T_{cell}, equals ambient temperature. The initial SOC decreases with decreasing temperature. The instantaneous SOC is calculated by subtracting the proportion of total battery charge removed by the battery current after a set time interval [5]. A popular approach to model batteries is through equivalent circuit models and here an adaptive circuit as seen in relevant literature, shown in Fig. 1 [5] will be used.

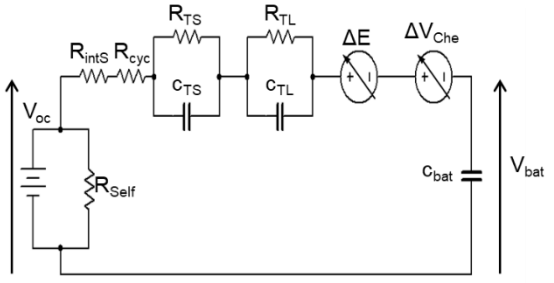

Fig. 1 Battery Equivalent Circuit [5]

R_{self} models the battery's self-discharge rate, which results from the electrolyte passing ions when the battery is stored [5]. This model presumes these losses to be negligible, since it focusses on the battery in closed-circuits. ΔE and ΔV_{Che} are small losses caused by battery chemistry relating to the battery's activation energy across the electrolyte interface [5]. Here these parameters are assumed negligible.

There is a time delay between a change in system current requirement and the corresponding change supplied battery current. This is accounted for by the RC networks in Fig. 1 and is dependent on SOC as given for Lithium by Equations 3, 4, 5 and 6, which are temperature independent [6].

$$R_{TS} = 0.3208e^{-29.14(SOC)} + 0.04669 \quad (3)$$

$$C_{TS} = -752.9e^{-13.51(SOC)} + 703.6 \quad (4)$$

$$R_{TL} = 6.603e^{-155.2(SOC)} + 0.04984 \quad (5)$$

$$C_{TL} = -6056e^{-27.12(SOC)} + 4475 \quad (6)$$

Variable R_{cyc} represents the aging loss in capacity with n charging cycle, given by Equation 7 [4].

$$R_{cyc} = 0.0015\sqrt{n} \quad (7)$$

A battery capacity correction factor F_{cc} is employed to account for battery storage losses, with t as the time in months that the battery spent in storage and T_{amb} is in Kelvin here [4].

$$F_{cc} = 1 - 1.544 \times 10^5 \exp\left(\frac{-40498}{8.3143\, T_{amb}}\right) t \quad (8)$$

The key battery parameter affected by changes in ambient temperature is the internal resistance R_{intS}. At low temperatures this increases because of the low kinetic energy of Lithium ions crossing the electrolyte material [7]. Increasing temperature can thus increase battery capacity for one battery cycle, as also indicated by Equation 2, but the cyclic loss is amplified, decreasing Q_{usable} [4]. The internal battery resistance is given by combining Equations 9 and 10 [5, 6]. Here T_{amb} is the battery's ambient temperature in degrees Celsius and R_{int0} is a reference value at the same SOC and an ambient temperature of 0°C.

$$R_{intS}(SOC) = -1.399 \times 10^{-5} \times T_{amb}^2 - 2.768 \times 10^{-4} \times T + R_{int0}(SOC) \quad (9)$$

$$R_{int0}(SOC) = 0.1562e^{-24.37(SOC)} + 0.07446 \quad (10)$$

2.2. BPMDC Motor Model:

A BPMDC motor is often modelled by an equivalent circuit comprising motor winding inductance L_a, winding resistance R_a, rotation speed ω, torque T_c, motor inductance L_f and induced electromotive force E_c as shown in Fig. 2 [8].

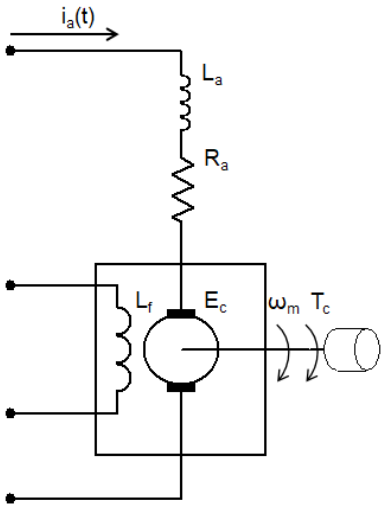

Fig. 2 BPMDC Motor Equivalent Circuit [9]

Variable i_a is the current drawn by the motor. The overall voltage required by the

motor is given by Equation 11. Equation 12 relates current and motor torque τ_D [8].

$$V_M = i_a R + L_a \frac{di}{dt} + k_\tau \omega \qquad (11)$$

$$\tau_D = k_\tau i_a \qquad (12)$$

Here k_τ is the motor torque constant. Equation 13 is the sum of the motor's load torque, τ_l, no-load torque τ_0 and angular acceleration multiplied by the inertia J [8].

$$\tau_D = \tau_l + \tau_0 + J \frac{d\omega}{dt} \qquad (13)$$

If the motor is controlled by a H-Bridge with a pulse-width modulation (PWM) switching scheme and duty ratio ρ. The motor current is related to the current drawn from the battery, i_{Mx}, by Equation 14 [9].

$$i_{Mx} = \rho i_a \qquad (14)$$

Thus, motor current is higher than the current drawn from the battery.

The temperature of the motor can be modelled using the equivalent circuit in Fig. 3 and Equation 15 [3].

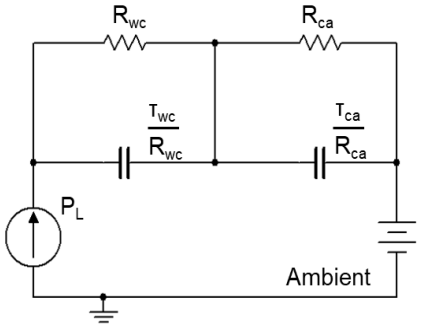

Fig. 3 BPMDC Motor Thermal Model [6]

$$T_w = \frac{R_{wc} P_M}{\tau_{wc} s + 1} + \frac{R_{ca} P_M}{\tau_{ca} s + 1} + T_{amb} \qquad (15)$$

This equation takes the motor power loss, as well as the winding-to-casing and the casing-to-ambient thermal time-constant into account. The motor power loss is given by Equation 16.

$$P_M = i_a^2 R + \frac{k_e \tau \omega}{k_\tau} + \frac{k_e \tau \omega^2}{k_\tau} \qquad (16)$$

Variable k_e relates to the term $k_\tau \omega$ in Equation 11. The winding resistance is temperature dependent according to Equation 17 [3].

$$R = R_0\big(1 + \psi(T_1 - T_0)\big) \qquad (17)$$

The resulting current dissipation in R implies that the BPMDC motor requires more current to maintain the same torque at higher temperatures. The torque constant k_τ and inductance L_a are varied in the same manner.

2.3. Robot Model:

The torque required to move the robot up an incline of θ assuming negligible aerodynamic force is given by Equation 18, as shown in Fig. 4. The robot tracks follow the outline of its main body and movable flippers, to allow climbing, can be seen at its sides.

$$\tau_l = (ma + \mu mg \cos\theta + mg \sin\theta) r \times \frac{1}{G\eta} \qquad (18)$$

Variable m is the robot mass, a is its acceleration, μ is the friction coefficient, r the wheel radius, g is gravity, G the gear ratio between motor and wheel and η is the motor efficiency. The wheels driven by the motors drive a pair of track and no-slip between the components is assumed.

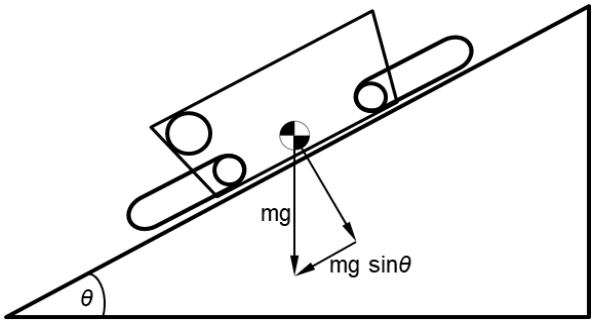

Fig. 4 Free Body Diagram

The torque in the robot's flippers is given by Equation 19.

$$\tau = \frac{m_l g l}{2} \times \frac{1}{G\eta} \qquad (19)$$

Here m_l is the load to be lifted and l its distance from the centre of rotation. Equations 18 and 19 can be used in conjunction with Equation 12 and 13 to model the current drawn by the robot motors during different operations.

The current drawn by on-board instrumentation is estimated through Equation 20 and assumed to remain constant with temperature.

$$I_{ob} = \left(I_{comp} + I_{sens}\right) \times (2 - \eta_{conv}) \qquad (20)$$

The factor $(2 - \eta_{conv})$ is included to account for on-board converter inefficiencies, as the robot uses a single battery power supply.

Overall current drawn by the electronic system on-board the robot is given by Equation 21.

$$i_{draw} = I_{Mt} + I_{Mf} + I_{Ma} + I_{ob} \qquad (21)$$

$I_{Mt}$is the current drawn by the track motors, I_{Mf} that drawn by the flippers and I_{ma} that drawn by the robot arm. This is then substituted for $i_{battery}$ in Equation 1 to allow for SOC and battery life estimation. Converter efficiency here is 0.86 (TRACO POWER TEL 30-24xx Series) and the duty ratio ρ is given by Equation 22.

$$\rho = \frac{V_{set} - 2.5}{2.5} \qquad (22)$$

Here V_{set} is the voltage signal between 0 and 5V sent to the robot by the remote operator, with 5V indicating maximum forward speed and 2.5V indicating zero speed.

3. Simulation Results:

A battery cell model powering two BPMDC motors, like that described above was implemented in MATLAB Simulink by Huria et al. in [10], see Fig. 5. The model here adapts parts of this with Equations 2 to 10 but combining R_{intS} and R_{cyc} with the assumption made that $n = 25$.

The simulated battery is made up of six 3.8V cells in series, to give a total Voltage of 22.8V, with a Capacity of 5.2 Ah. To account for storage losses after 18 months of storage the capacity correction factor from Equation 8 is employed to give a remaining battery capacity of about 4.2 Ah. Lookup tables (LUT) containing values at 6 SOC breakpoints for R_{TS}, C_{TS}, R_{TL} and C_{TL}, assuming an initial SOC of one, are computed. The no-load torque τ_0 was calculated to be about 10m Nm. The components that make up the BPMDC motor's equivalent circuit are varied with temperature following the behaviour of Equation 17 assuming copper windings and a Neodymium permanent magnet with R of 0.103Ω and ψ as 0.0039pcK^{-1}. The no load torque is given by the torque constant multiplied by the no load current. The motors are 94% efficient and the main track gear ratio G is 156. Motor torque is computed from Equation 18 and 13 assuming operation at zero-degree incline and a rubber on asphalt friction coefficient of 0.7. The battery current is then ultimately obtained from Equation 21.

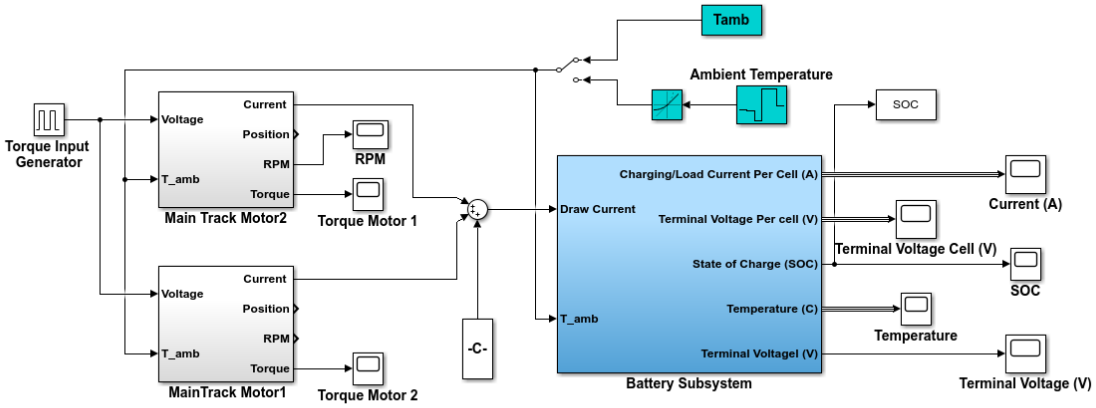

Fig. 5 Full Simulink Model

At a precomputed value for R_{intS} at 20°C, simulation has shown that T_{cell} does not increase by more than approximately 4°C when discharging at an ambient temperature of 20°C. Because of this it is assumed that T_{cell} is equal to T_{amb}, which results in SOC_0 of approximately one according to Equation 2. Because of this is assumption it is possible to add a LUT with values for R_{intS} at temperatures between -20°C and 100°C in 20°C increments. Simulation results for the model described above at varying ambient temperatures at constant torque are shown in Fig. 6.

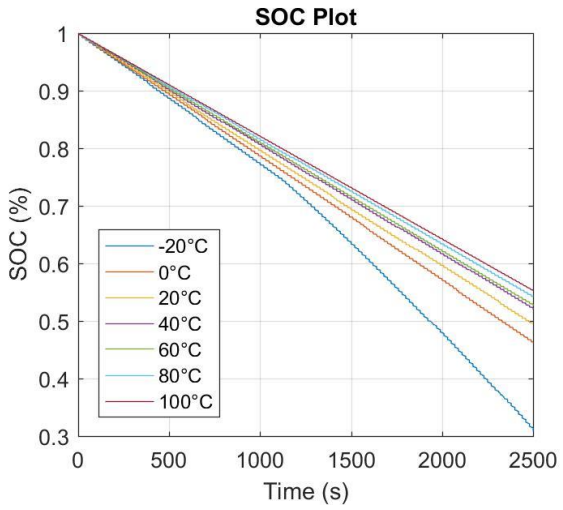

Fig. 6 SOC at Ambient Temperature Change

The remaining SOC at any time t varies significantly as the temperature varies from 20°C and further that the discharge is approximately linear. As was expected the battery depletes faster at lower temperatures.

The discharge (SOC) gradients of the graphs in Fig. 6 are given in Table 1.

Temperature ($°C$)	**SOC Gradient (s^{-1})**
-20	-2.8×10^{-4}
0	-2.5×10^{-4}
20	-2.1×10^{-4}
40	-1.6×10^{-4}
60	-1.3×10^{-4}
80	-0.9×10^{-4}
100	-0.5×10^{-4}

Table 1 SOC gradient at varying temperature

From the values above the average change in SOC gradient per 20°C temperature decrease obtained through simulation is about $0.33 \times 10^{-4} s^{-1}$.

With the ambient temperature set to 20°C the BPMDC motor torque is varied between 0Nm and 0.35Nm. The results are plotted in Fig. 7.

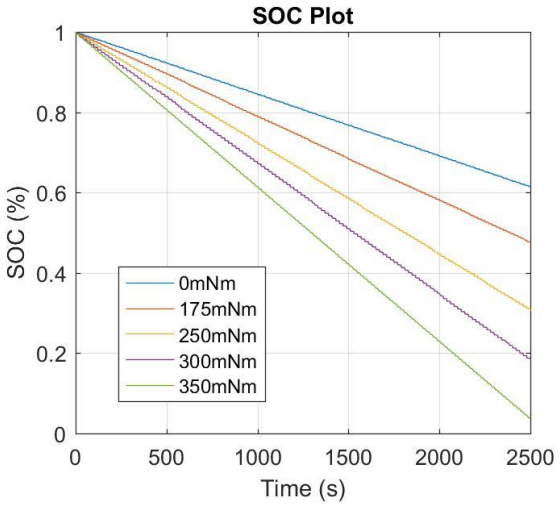

Fig. 7 SOC at varying Motor Torque

As expected, the battery SOC decreases faster as the motor torque increases. The graphs are also approximately linear. Observed gradients are given in Table 2.

Torque (mNm)	SOC Gradient (s^{-1})
175	-2.0×10^{-4}
250	-2.8×10^{-4}
300	-3.4×10^{-4}
350	-3.8×10^{-4}

Table 2 SOC gradient at varying torque

The average gradient change of the graphs in Fig. 7 per 0.05Nm increase in torque is thus 0.5×10^{-4} s^{-1}. It follows that when the batteries are discharged under varying torque at low temperatures, the SOC will deplete at a higher rate still.

To compensate for amplified discharge rates to maintain battery life at varying temperatures and allow consistent SOC estimations, a mechanism to adjust current draw depending on ambient temperature and torque output is needed. Further effects of this are reduced battery life cycle losses from high temperature cycling and improved robot safety from additional battery monitoring.

The results in Fig. 6 imply that when the ambient temperature increases by 20°C, a discharge current reduction of about 15.7% is required. Similarly, for the torque a reduction of 14.7% per 50mNm is needed.

Since SOC is generally not measured directly, alternate quantity needs to be measured [11]. Two SOC dependent quantities are the battery cell voltage and internal resistance. Fig. 8 shows the behaviour of cell voltage under 0Nm motor torque and 20°C ambient temperature. For safety reasons and to ensure the battery will maintain its ability to be recharged, Lithium batteries should not be fully discharged. The battery cells employed are 3.8V and a remaining cell voltage of about 3V is recommended [12].

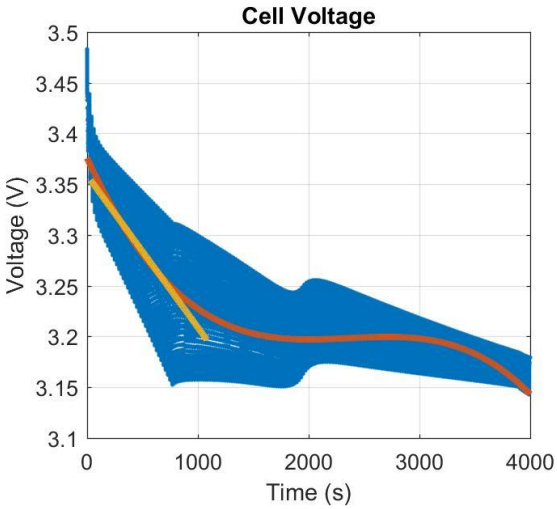

Fig. 8 Change in Cell Voltage

The blue points indicate the fluctuation in battery voltage under pulse discharge at different sampling times and the orange line is a third order polynomial approximating the voltage decrease over time, with an average gradient of about -5.8×10^{-5} Vs^{-1}. This is

observed as approximately linear between 30s and 1080s. The gradient of the linear approximation represented by the yellow line is $-0.15\times10^{-5}Vs^{-1}$. Further it can be seen that battery voltage remains approximately constant between about 1200s and 3000s. If the data in Fig. 8 is represented by a first order polynomial its gradient is about $-3.5\times10^{-5}Vs^{-1}$. According to the observations from Fig. 8, the battery cell voltage drops down to 3.4V quickly and depletes to about 3.2V after 2000s.

4. Experimental Results:

The validity of the theoretical model was assessed through an experiment using the robot hardware. A RapidCharge LiPo 6S1P battery is connected to two Maxon RE50 BPMDC motors via a RoboClaw motor controller and discharged at two ambient temperatures, 20°C and 30°C. The tested motor load torque is 0 Nm and $\tau_0 = 10$mNm for a duration of thirty minutes or 1800s, to ensure it does not deplete excessively. The motors are tested at full speed and then with a 15% reduction in motor current draw. The battery cell voltage is measured continuously with a Rapid 318 DMM voltmeter of 0.1V accuracy. The battery resistance is measured initially and after test completion. All tests are executed on one battery. The measured initial and final battery voltages are given in Table 3 and the internal resistances in Table 4.

$\boldsymbol{Voltage\ (V)}$	$\approx \mathbf{20°C}$	$\approx \mathbf{30°C}$
$\boldsymbol{V_{initial} \pm 0.1V}$	22.6	22.6
$\boldsymbol{V_{final} \pm 0.1V}$	22.4/22.4	22.5/22.6

Table 3 Battery Voltage

$\boldsymbol{R\ (\Omega)}$	$\approx \mathbf{20°C}$	$\approx \mathbf{30°C}$
$\boldsymbol{R_{initial}}$	≈ 0.012	≈ 0.0055
$\boldsymbol{R_{final}}$	$\approx 0.04/0.03$	$\approx 0.018/0.016$

Table 4 Internal Battery Resistance

The non-compensated (nc) and compensated (c) per-cell voltage gradients with respect to time are given in Table 5. Cell voltage test results were generally within an order of magnitude of the values obtained through simulation, whereas the observed internal battery resistance was within 50 percent of the calculated values.

$\boldsymbol{Test}$	$\boldsymbol{Observed}$
$\boldsymbol{nc\ 20°C}$	-4.0×10^{-5}
$\boldsymbol{c\ 20°C}$	-3.4×10^{-5}
$\boldsymbol{nc\ 30°C}$	-1.7×10^{-5}
$\boldsymbol{c\ 30°C}$	0

Table 5 Measured Gradients

The voltage drops in Table 4 were observed between 750 and 1000 seconds of test runtime, the batteries did generally not deplete further before the end of each test after 1800s. This verifies the behaviour of the third order polynomial shown in Fig. 8, where the cell voltage depletes quickly for about 1100s and then plateaus until about 3000s of simulation runtime.

At 20°C the compensation has reduced the battery's depletion rate, which follows the theory, since a lower motor speed results in a lower current draw. However, there is a significant error between the simulated and the observed cell voltages. An explanation for the observed differences is battery storage loss from aging. The battery age may be more than the estimated 18 months.

This and storage temperature fluctuations would further affect the values computed through Equation 8 and hence the battery's capacity and internal resistance. The assumption that the initial battery SOC is one, regardless of ambient temperature, is another potential source of error. Initial SOC error is amplified further by storage loss, see Equation 8. One important parameter the simulation seems to overestimate is the no-load BPMDC motor current draw. The observed motor current was about 30% lower than that in the model in Fig. 5. This may be caused by the assumed linear relationship between the motor current and torque and the neglected temperature dependence of the torque constant [9]. Temperature effects on motor winding resistance and inductance also affect motor current draw and the simple linear model used in Equation 17 may not account for these sufficiently. The type of battery model employed here has previously been shown to have error without parameter adjustment [13]. The accuracy can be improved by the application of extended Kalman filters on the battery equivalent circuit components [13]. To show how the battery model improves with parameter adjustment a parametric sensitivity test was carried out on the Simulink model, where the equivalent circuit component values are doubled. The results of this are shown in Fig. 9. The voltage gradient of the yellow line here is about -0.33×10^{-5}Vs and hence closer to the observed values.

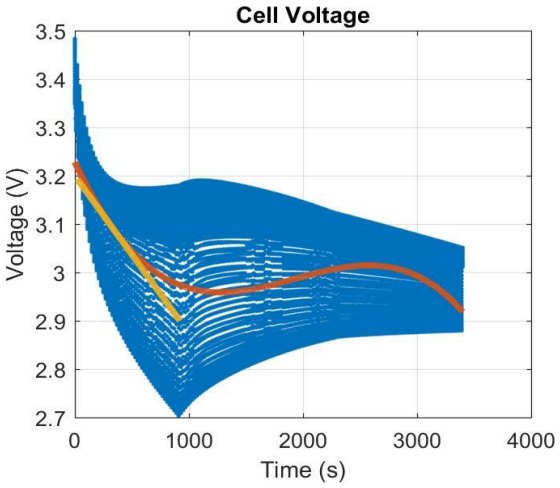

Fig. 9 Parametric Sensitivity Test

5. Conclusion:

An attempt to model battery SOC at varying temperatures was made. Since the compensation mechanism described above has been shown to result in decreased battery depletion rates, the general theory behind the simulated model is confirmed. However, a discrepancy between theoretical and experimental results is observed. Likely explanations for this include battery storage loss, but also uncertainties introduced by the various assumptions made to construct the model and simulate it successfully. Simulation has reinforced the expected behaviour of Lithium Batteries and BPMDC motors and the increase in internal battery resistance with decreasing battery state-of-charge has been shown both theoretically and experimentally. The behaviour of Lithium battery cell voltage during discharge was verified.

Further work on the model described may include more extensive system testing under varying motor load torques and wider temperature ranges. Obtained results could then be used to adjust the theoretical model to yield accurate state-of-charge estimations.

References:

[1] J. Larminie and J. Lowry, *Electric vehicle technology explained*, 2nd ed. Hoboken, N.J.: Wiley, 2012.

[2] C. Julien, A. Mauger, K. Zaghib and A. Vijh, *Lithium Batteries Science and Technology*. Switzerland: Springer, 2016.

[3] R. Pantonial, A. Kilantang and B. Buenaobra, "Real time thermal estimation of a Brushed DC Motor by a steady-state Kalman filter algorithm in multi-rate sampling scheme", in *TENCON 2012 - 2012 IEEE Region 10 Conference*, Cebu, Philippines, 2012.

[4] O. Erdinc, B. Vural and M. Uzunoglu, "A dynamic lithium-ion battery model considering the effects of temperature and capacity fading", in *2009 International Conference on Clean Electrical Power*, Capri, 2009, pp. 383-386.

[5] S. Wijewardana, R. Vepa and M. Shaheed, "Dynamic battery cell model and state of charge estimation", *Journal of Power Sources*, vol. 308, pp. 109-120, 2016.

[6] M. Chen and G. Rincón-Mora, "Accurate Electrical Battery Model Capable of Predicting Runtime and I–V Performance", *IEEE Transactions on Energy Conversion*, vol. 21, no. 2, pp. 504-511, 2006.

[7] L. Liao, P. Zuo, Y. Ma, X. Chen, Y. An, Y. Gao and G. Yin, "Effects of temperature on charge/discharge behaviors of LiFePO4 cathode for Li-ion batteries", *Electrochimica Acta*, vol. 60, pp. 269-273, 2012.

[8] A. Yildiz, "Electrical equivalent circuit based modeling and analysis of direct current motors", *International Journal of Electrical Power & Energy Systems*, vol. 43, no. 1, pp. 1043-1047, 2012.

[9] N. Mohan, T. Undeland and W. Robbins, *Power Electronics*, 3rd ed. Hoboken, NJ: Wiley, 2003.

[10] T. Huria, M. Ceraolo, J. Gazzarri and R. Jackey, "High fidelity electrical model with thermal dependence for characterization and simulation of high power lithium battery cells", in *2012 IEEE International Electric Vehicle Conference (IEVC)*, Greenville, 2012.

[11] M. Berecibar, I. Gandiaga, I. Villarreal, N. Omar, J. Van Mierlo and P. Van den Bossche, "Critical review of state of health estimation methods of Li-ion batteries for real applications", *Renewable and Sustainable Energy Reviews*, vol. 56, pp. 572-587, 2016.

[12] K. Ng, C. Moo, Y. Chen and Y. Hsieh, "Enhanced coulomb counting method for estimating state-of-charge and state-of-health of lithium-ion batteries", *Applied Energy*, vol. 86, no. 9, pp. 1506-1511, 2009.

[13] Y. Diab, F. Auger, E. Schaeffer and M. Wahbeh, "Estimating Lithium-Ion Battery State of Charge and Parameters Using a Continuous-Discrete Extended Kalman Filter", *Energies*, vol. 10, no. 8, p. 1075, 2017.